

Poleward shift in Indian summer monsoon low level jetstream under global warming

S. Sandeep · R. S. Ajayamohan

Received: 17 March 2014 / Accepted: 12 July 2014 / Published online: 24 July 2014
© Springer-Verlag Berlin Heidelberg 2014

Abstract The low level jetstream (LLJ) transports moisture from the surrounding Oceans to Indian land mass and hence an important component of the Indian summer monsoon (ISM). Widening of tropical belt and poleward shifts in mid-latitude jetstreams have been identified as major impacts of global warming on large-scale atmospheric dynamics. A general northward shift in ISM circulation has been suggested recently, based on the Coupled Model Inter-comparison Project (CMIP5) simulations. Here, we investigate the current and projected future changes in LLJ in observations as well as the coupled model (CMIP3/CMIP5) simulations. A poleward shift in the monsoon LLJ has been detected both in the observations and coupled model simulations. The poleward shift is also reflected in the future projections in a warming scenario, with the magnitude of shift depending on the degree of warming. Consistent with the LLJ shift, a drying (wet) trend in the southern (northern) part of the western coast of India is also observed in the last three decades. Further analysis reveals that enhanced land-sea contrast resulted in a strengthening of the cross-equatorial sea level pressure gradient over Indian Ocean, which in turn resulted in the northward shift of the zero absolute vorticity contour from its climatological position. The poleward shift in zero absolute vorticity contour is consistent with that of LLJ core (location of maximum low-level zonal winds). Possible uncertainties in the results are discussed in the context of known model biases and ensemble sample sizes. These results assume significance in the context of the concerns over ecologically fragile Western Ghats region in a warming scenario.

Keywords Indian monsoon · Low level jet · Global warming · Hydrological cycle · Western Ghats

1 Introduction

The agrarian based livelihood of the densely populated south-Asian continents crucially depends on the summer monsoon rainfall (Gadgil and Gadgil 2006). Hence, the impact of climate change on the Indian summer monsoon (ISM) circulation and precipitation pattern assumes significance. A major change that is observed in the ISM in recent decades is a summer drying over central India in the second half of the twentieth century which was attributed to anthropogenic aerosol related radiative effects (Bollasina et al. 2011). The aerosol effect on ISM circulation is a matter of ongoing debate (Lau and Kim 2006; Nigam and Bollasina 2010). Increase in the atmospheric stability in a warming climate was also proposed as a cause of the weakening of the ISM circulation (Krishnan et al. 2013; Rajendran et al. 2012). Increased frequency in the drought events over India was proposed under an increased regional aerosol emission scenario (Ramanathan et al. 2005). However, the summer drying trend over India has declined in the recent decade (Turner and Annamalai 2012). At the same time, the character of ISM precipitation was found to be changing towards an increased frequency of extreme events (Goswami et al. 2006; Ajayamohan and Rao 2008). The increase in the precipitation extremes was found to be associated with a corresponding increase in the synoptic activity over India (Ajayamohan et al. 2010).

An important component of ISM is the low level jetstream (LLJ; Joseph and Raman 1966; Findlater 1969) that transports moisture from the Indian Ocean to the South Asian land mass. By analyzing the NCEP-NCAR

S. Sandeep · R. S. Ajayamohan (✉)
Center for Prototype Climate Modeling, New York University
Abu Dhabi, Abu Dhabi, UAE
e-mail: ajayanrs@gmail.com; Ajaya.Mohan@nyu.edu

reanalysis data, Joseph and Simon (2005) suggested a weakening trend in the LLJ strength, which was in tune with the intraseasonal rainfall variability (Joseph and Sijikumar 2004). Consistent with the weakening of LLJ, a weakening in the upper level circulation, known as Tropical Easterly Jet (TEJ), is also reported (Sathiyamoorthy 2005; Abish et al. 2013). Few coupled general circulation model (CGCM) simulations with enhanced green house gas (GHG) concentrations also report a weakening ISM circulation (May 2002; Stowasser et al. 2009; Kitoh et al. 2013).

Despite the advances in climate modeling, accurate simulation of the main features of ISM is still a challenge for CGCMs (Sperber et al. 2013). Although, an overall improvement in the simulation of ISM is exhibited by many models that participate in the fifth phase of Coupled Model Inter-comparison Project (CMIP5; Taylor et al. (2011)) over its predecessors in CMIP3 (Meehl et al. 2007), no single model simulates all features of ISM realistically (Sperber et al. 2013). Therefore the conclusions from CGCM simulations need to be drawn carefully. The cold bias in Sea Surface Temperature (SST) during pre-monsoon season over the Arabian Sea and the resultant weaker moisture transport to the land cause a dry bias over India in most of the CMIP3 and CMIP5 models (Levine et al. 2013; Marathayil et al. 2013). While most models have difficulty in simulating the seasonal mean precipitation over India, greater fidelity is seen in the simulation of winds (Sperber et al. 2013). Most of the CMIP3 models do not show any considerable change in the mean ISM precipitation under future warming scenarios (Kumar et al. 2011; Turner and Annamalai 2012). However, some of the CGCM experiments with enhanced GHG concentrations show increased ISM precipitation (Ashrit et al. 2003; Meehl and Arblaster 2003; Ashrit et al. 2005). In contrast with CMIP3, the future projections of CMIP5 models show a strong wet trend over India during summer (Kitoh et al. 2013; Menon et al. 2013a). Wang et al. (2013) also reports an intensification of northern hemisphere summer monsoon in recent decades.

In light of the suggested wet trend of monsoon in a global warming scenario, the changes in the strength and location of LLJ assume significance. Whether the weakening of LLJ seen in NCEP/NCAR reanalysis products (Joseph and Simon 2005) reflects in the projected future warming scenarios is an interesting question which needs thorough investigation. Another important aspect is whether the dynamics of LLJ is consistent with the weakening trend. The higher fidelity of the climate models in simulating the mean winds as compared to precipitation provide more confidence in using CMIP3 and CMIP5 model simulations in studying LLJ changes in future decades. Poleward shifts in sub-tropical jetstream and mid-latitude storm tracks

(Fu and Lin 2011), and a widening of tropical belt (Fu 2006; Seidel and Randel 2007) have been observed and identified as major impacts of global warming on large-scale atmospheric circulations. A shift in LLJ strength and location can have strong implications on South-Asian circulation and precipitation patterns. Such a shift in LLJ location has not been detected in the observations and CGCMs so far, although few studies report a northward shift in ISM circulation (May 2002; Ashrit et al. 2003; Turner et al. 2007; Menon et al. 2013b).

Our main objective is to examine the LLJ characteristics in CMIP3/CMIP5 model simulations and in observed precipitation/wind data products. We specifically investigate the changes in LLJ strength and location in future projection. What is the projected magnitude of LLJ shift and strength by the end of the century? Further, the underlying dynamics in LLJ changes in future decades is discussed. The implications of the projected changes in LLJ are also examined.

Data and methodology to find the LLJ trends are discussed in Sect. 2. Detection of poleward shift in LLJ and its dynamics are explained in Sects. 3, 4 respectively. The uncertainties in the results are discussed in Sect. 5. Finally, a concluding summary and discussion is provided in Sect. 6.

2 Data and methods

The historical All Forcing (AF) and different Representative Concentration Pathways (RCP; Moss et al. (2010)) simulations of CMIP5 are used in this study. Climate of the twentieth century (20c3 m) as well as Special Reports on Emission Scenarios (SRES) (Nakicenovic et al. 2000) A1B, A2, and B1 simulations of CMIP3 are also utilized. The details of CMIP5 climate models and experiments used in this study are provided in Table 1. In the case of CMIP3, we used five models (miroc3_2_medres, mpi_echam5, gfdl_cm2_0, gfdl_cm2_1, mri_cgcm2_3_2a) of which latter four are found to simulate ISM precipitation reasonably well (Turner and Annamalai 2012). We use monthly mean precipitation, surface skin temperature (TS), mean sea level pressure (PSL), and zonal (U) as well as meridional (V) wind fields from the CGCM simulations. TS over Oceans is taken as a proxy for SST in climate model simulations. The monthly mean meridional oceanic heat transport from RCP8.5 experiments is also used in this study. The ensemble mean of meridional oceanic heat transport is generated using slightly different subset of CMIP5 models (as indicated by “*” in Table 1 and three additional models—CMCC-CM, CMCC-CMS, and MRI-ESM1), as all models do not output this parameter. Also, monthly mean wind fields from ERA-Interim Reanalysis (ERA-I; Dee

Table 1 CMIP5 models and experiments used in this study

Model/experiment	RCP2.6	RCP4.5	RCP6.0	RCP8.5
ACCESS1-0	Not available (N)	Available (Y)	N	Y*
ACCESS1-3	N	N	N	Y*
bcc-csm1-1	Y	Y	Y	Y
bcc-csm1-1 m	Y	Y	Y	Y
CanESM2	Y	Y	N	Y
CCSM4	Y	Y	Y	Y
CESM1-BGC	N	Y	N	Y
CESM1-CAM5	Y	Y	Y	Y
CMCC-CESM	N	N	N	Y*
CNRM-CM5	Y	Y	N	Y*
CSIRO-Mk3-6-0	N	N	Y	Y
FGOALS-g2	N	Y	N	Y
GFDL-CM3	Y	Y	Y	Y
GFDL-ESM2G	Y	Y	Y	Y
GFDL-ESM2 M	Y	Y	Y	Y
GISS-E2-H	Y	Y	Y	Y
GISS-E2-H-CC	N	Y	N	Y
GISS-E2-R	Y	Y	Y	Y
GISS-E2-R-CC	N	Y	N	N
HadGEM2-AO	Y	Y	Y	Y
HadGEM2-CC	N	Y	N	Y
HadGEM2-ES	Y	Y	Y	Y
inmcm4	N	Y	N	Y
IPSL-CM5A-LR	Y	Y	Y	Y*
IPSL-CM5A-MR	Y	Y	Y	Y*
IPSL-CM5B-LR	N	Y	N	N*
MIROC5	Y	Y	Y	Y
MIROC-ESM-CHEM	Y	Y	Y	Y
MIROC-ESM	Y	Y	Y	Y
MPI-ESM-LR	Y	Y	N	Y*
MPI-ESM-MR	Y	Y	N	Y*
MRI-CGCM3	Y	Y	Y	Y*
NorESM1-M	Y	Y	Y	Y*
NorESM1-ME	Y	Y	Y	Y*
Total # of models	23	31	20	32

* Indicates the models that are used to generate ensemble mean of Oceanic meridional heat transport

et al. (2011)) and monthly mean precipitation from Asian Precipitation—Highly-Resolved Observational Data Integration Towards Evaluation of Water Resources (APHRO-DITE; Yatagai et al. (2012)) were used. The monthly mean Hadley Center SST1.1 (HadISST; Rayner et al. (2003)) is used to estimate the model bias in Arabian Sea SST. We have also used Wave and Anemometer based Sea surface Wind (WASWind; Tokinaga and Xie (2011)) data product to determine the changes in LLJ during 1951–2010 period.

2.1 Detection of LLJ shift

The coarse resolution of some CMIP5 CGCMs can result in errors in the detection of LLJ shift. Hence, linear interpolation of the model data is carried out for coarse resolution models to a finer $1^\circ \times 1^\circ$ resolution. However, few model outputs from the CMIP5 suite (e.g. CCSM4, CESM1-CAM5, MRI-CGCM3) already comes in high resolution. Errors caused by linear interpolation will be minimal in such models (biases are discussed in Sect. 5). All the analyses are done for the June–September (JJAS) season. We rely on a three-pronged analysis technique to calculate LLJ shift to ensure robustness of the results.

1. Dynamically, LLJ maxima is located poleward of zero absolute vorticity contour ($\eta = 0$; Tomas and Webster (1997); see Sect. 4 for details). Therefore the location of $\eta = 0$ contour over the Arabian Sea can be considered as a proxy for the LLJ location. The maximum poleward latitudinal location of zero absolute vorticity ($\Phi_{\eta=0}$) over the Arabian Sea (50°E – 70°E) is determined for all models.
2. The LLJ core is defined as the location of maximum JJAS zonal wind at 850 hPa (U850) over the Arabian Sea (50°E – 70°E , 5°N – 25°N). The latitudinal location of U850 maximum ($\Phi_{U_{\max}}$) is determined for all models.
3. The monsoon winds change its direction from south-easterly to south-westerly, close to the equator. We find the latitude at which the zonal mean (50°E – 70°E) U850 change its direction from easterly to westerly ($\Phi_{U850=0}$), in a similar way as $\Phi_{\eta=0}$.

Often $\eta = 0$ or $U850 = 0$ may not lie exactly on a model grid point. In such instances we find $\Phi_{\eta=0}$ or $\Phi_{U850=0}$ by linearly interpolating between two adjacent latitudinal grids where the transition from negative to positive value takes place, as follows

$$\Phi_{x=0} = \Phi_{x_-} + \left(\frac{-x_-}{x_+ - x_-} \right) (\Phi_{x_+} - \Phi_{x_-})$$
, where x can be η or U850. Φ_{x_-} and Φ_{x_+} are the latitudes where the transition of x from negative (x_-) to positive (x_+) value occurs.

In all the three cases, the annual anomaly in Φ_x is calculated as $\Phi'_x = \Phi_x - \bar{\Phi}_x$ where x can be $\eta = 0$, U_{\max} or $U850 = 0$ and $\bar{\Phi}_x$ is the reference climatology (1981–2000) of Φ_x .

2.2 Trends and significance

The temporal trends are calculated using least square linear regression. The correlations are calculated using Pearson correlation technique. Statistical significance is estimated using two-tailed t test. While calculating the t value for correlations and trends, the number of degrees of freedom

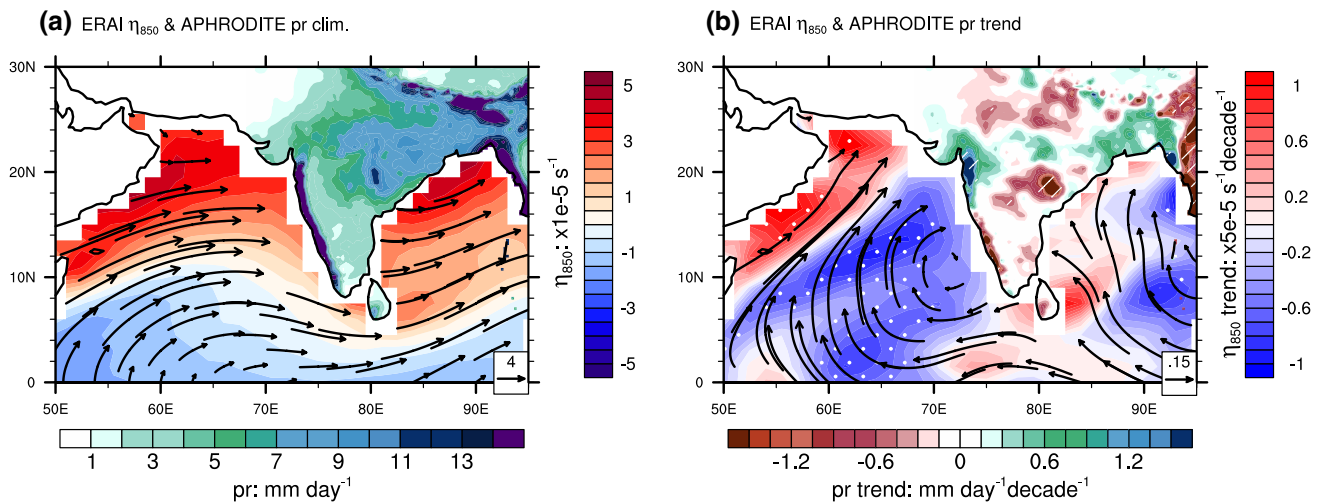


Fig. 1 **a** Climatological JJAS mean (1981–2000) oceanic winds at 850 hPa, (vectors; m s^{-1}), absolute vorticity (shading over oceans; $1 \times 10^{-5} \text{ s}^{-1}$) and land precipitation (mm day^{-1}) and **b** linear trends (1979–2007) in JJAS mean winds (vectors, $\text{m s}^{-1} \text{ decade}^{-1}$), absolute vorticity (shading over oceans; $5 \times 10^{-5} \text{ s}^{-1} \text{ decade}^{-1}$) and land

precipitation ($\text{mm day}^{-1} \text{ decade}^{-1}$). Winds are from ERA-Interim and precipitation from APHRODITE. Stippling (*dashes*) show regions with statistically significant ($p < 0.05$) trends in zonal winds (precipitation)

(*dof*) were adjusted for the lag 1 autocorrelation (r_1), when r_1 was significant at the 5 % level, as $n' = n(1-r_1)/(1+r_1)$, where n' is the adjusted *dof* and n is the original *dof*. The trends for ERAI U850 and APHRODITE precipitation are calculated for the period of combined availability of both data (1979–2007). The trends for historical AF simulations are calculated for 1901–2005 period and those for RCP simulations are calculated for 2006–2099 period, unless otherwise specified. The trends for CMIP3 20c3 simulations are calculated for 1901–2000 and those for SRES scenarios are computed for 2001–2099 period.

3 Poleward shift in LLJ

The interaction of monsoon LLJ with Western Ghats orography produces copious amount of rainfall on the west coast of India. The low-level (850 hPa) monsoon winds and land-precipitation over Indian land region underlines this fact (Fig. 1a), consistent with previous studies (Xie et al. 2006; Krishnan et al. 2013). Positive (negative) vorticity is seen on the northern (southern) flanks of the LLJ, in line with the concept of LLJ as a convergence-divergence couplet (Tomas and Webster 1997). Decreasing (increasing) trends in the rainfall over southern (northern) parts of the Western Ghats is observed since 1901 (Guhathakurta and Rajeevan 2008). A linear trend analysis of APHRODITE precipitation over land shows north–south wet-dry pattern over western India (Fig. 1b). Analysis of ERAI winds shows a corresponding change in monsoon low-level flow, suggesting a northward shift in the LLJ. Consistent with

the changes in the winds, a weakening (strengthening) of the vorticity over the southern (northern) Arabian Sea is found. The precipitation trend pattern in our analysis is in line with the centennial trend observed by Guhathakurta and Rajeevan (2008). It shall be noted that WASWind, a surface wind data product derived from ship observations also shows a shift in LLJ of similar magnitude in last six decades (figure not shown). The weakening of the monsoon south of 16°N is attributed to the weakening of south-westerlies in response to increased atmospheric static stability (Rajendran et al. 2012). However, their analysis did not explain why the atmospheric stability increased only south of 16°N . The dry trend south of 16°N and the corresponding wet trend north of 16°N suggest the possibility of a poleward shift in LLJ in observations. It may be noted that these trends are derived from last three decades of reliable observations after the satellite era.

Further, the ensemble of climate model simulations in CMIP5 is examined to understand the changes the LLJ and corresponding precipitation changes in a global warming scenario. The climatological mean low-level winds and precipitation pattern in historical AF experiment is shown in Fig. 2a. The overall mean structure of LLJ and enhanced precipitation over Western Ghats is simulated in the AF simulations. However, the fine scale features of the precipitation pattern are not resolved in AF simulations as in high resolution APHRODITE observations. The trend patterns in the winds show strengthening (weakening) over the northern (southern) Arabian Sea (Fig. 2b). The changes in vorticity also show a broad area of weakening between 10 and 16°N and a region of strengthening between 16 and

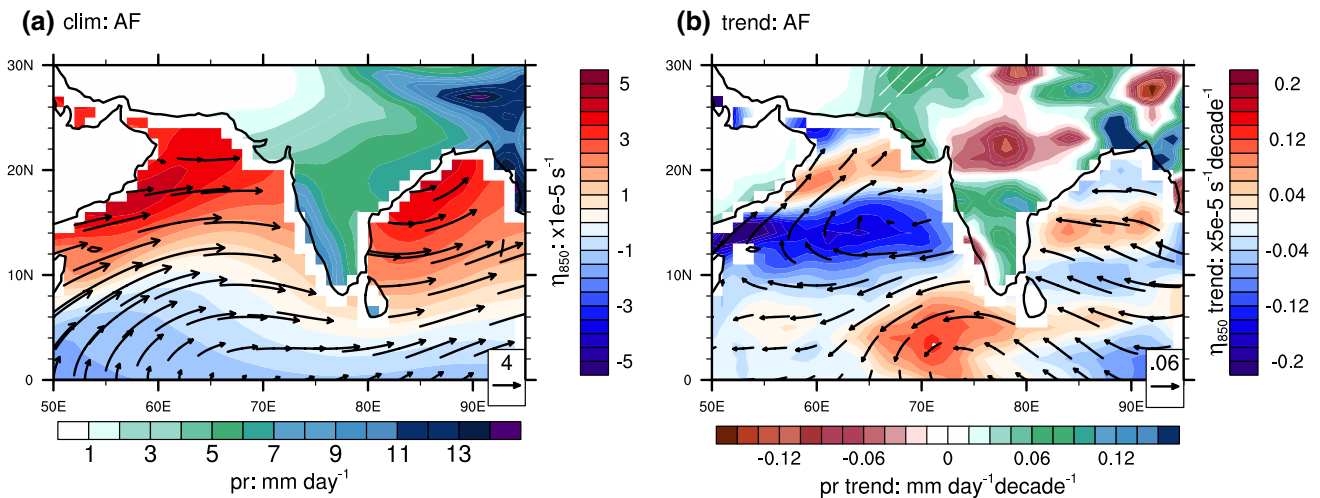


Fig. 2 **a** Same as Fig. 1a, except for ensemble mean of historical AF simulations (1981–2000) and **b** linear trend (1979–2005) for AF ensemble

20°N over the Arabian Sea. A drying trend south of 16°N and wet trend over north-west India is consistent with the changes in the low level wind flow. A direct comparison of the observed winds and precipitation trends (Figs. 1b, 2b) reveals the systematic errors of the climate models, especially in precipitation. The limitation of coarse resolution CGCMs in simulating monsoon precipitation is discussed before (Sperber et al. 2013). However, consistency in trends between precipitation and low-level winds in AF simulations gives confidence in assessing the trends of CGCMs in the future projections.

It would be interesting to investigate whether the trends seen in the late twentieth century simulations intensifies in the future projections. The linear trend analysis on oceanic winds, absolute vorticity, and land precipitation for the 2006–2099 projections of CGCMs is repeated on ensemble simulations based on various RCP scenarios (Fig. 3a–d). The LLJ seems to be strengthening (weakening) north (south) of ~15°N over the Indian Ocean domain suggesting a poleward shift of LLJ in a warming scenario. The weakening (strengthening) of absolute vorticity over southern (northern) Arabian Sea is consistent with the corresponding changes in the LLJ. The trend pattern for the winds seen in AF ensemble is found to be getting stronger with stronger emission scenarios. This indicates that the degree of the poleward shift in the ISM low level circulation depends on the magnitude of external forcing. It is noteworthy that the trends in U850 are statistically significant ($p < 0.05$) for various RCP scenario simulations, except that RCP2.6 show insignificant trends over southern Arabian Sea. Interestingly, the trends in future precipitation pattern do not reflect the pattern of shift in low level wind flow. This could be due to the fact that, in a warming scenario, the increased moisture transport might offset the weakening of the winds,

as suggested in recent studies (Kitoh et al. 2013; Menon et al. 2013a). Also, we highlight the fact that the precipitation simulations of the CGCMs are not as reliable as winds (see Fig. 13), with the ensemble mean precipitation and U850 yielded pattern correlations of 0.9 and 0.98 respectively with observations (Sperber et al. 2013). The deficiencies in the precipitation simulation by the CGCMs coupled with their coarse resolution pose a hindrance to determine fine-scale features of changes in the regional precipitation, especially over the narrow belt of Western Ghats orography. Future projection by a high resolution (~20 km) CGCM yielded a reduction (enhancement) in rainfall over the west coast of India south (north) of 16°N (Rajendran et al. 2013). Thus, extreme caution needs to be taken while interpreting the orographic precipitation trends over Western Ghats in coarse-resolution CGCMs. On the other hand, the chances of increased precipitation over north-west India are high, with the poleward shift in the monsoon low level winds coupled with enhanced evaporation in a warmer atmosphere.

An estimate of the magnitude of latitudinal shift in LLJ is made from the $\Phi_{\eta=0}'$ (based on zero absolute vorticity) and $\Phi_{U_{max}}'$ (based on U850 maximum) from the historical AF and RCP scenario experiments (Fig. 4). $\Phi_{\eta=0}'$ has experienced a slight poleward shift in RCP2.6 ensemble means (Fig. 4a). While there is no trend in $\Phi_{\eta=0}'$ in the AF ensemble when the whole twentieth century is considered, a slight poleward trend is seen in the last three decades of AF simulations. The ERAI reanalysis (yellow line, Fig. 4a) also show a strong and significant trend of 0.3 degrees decade⁻¹ in $\Phi_{\eta=0}'$ in the 34 year period. The linear trends in $\Phi_{\eta=0}'$ are also statistically significant for RCP4.5, RCP6.0, and RCP8.5, with values of 0.07, 0.09, and 0.15 degrees decade⁻¹ respectively (Fig. 4b). The core

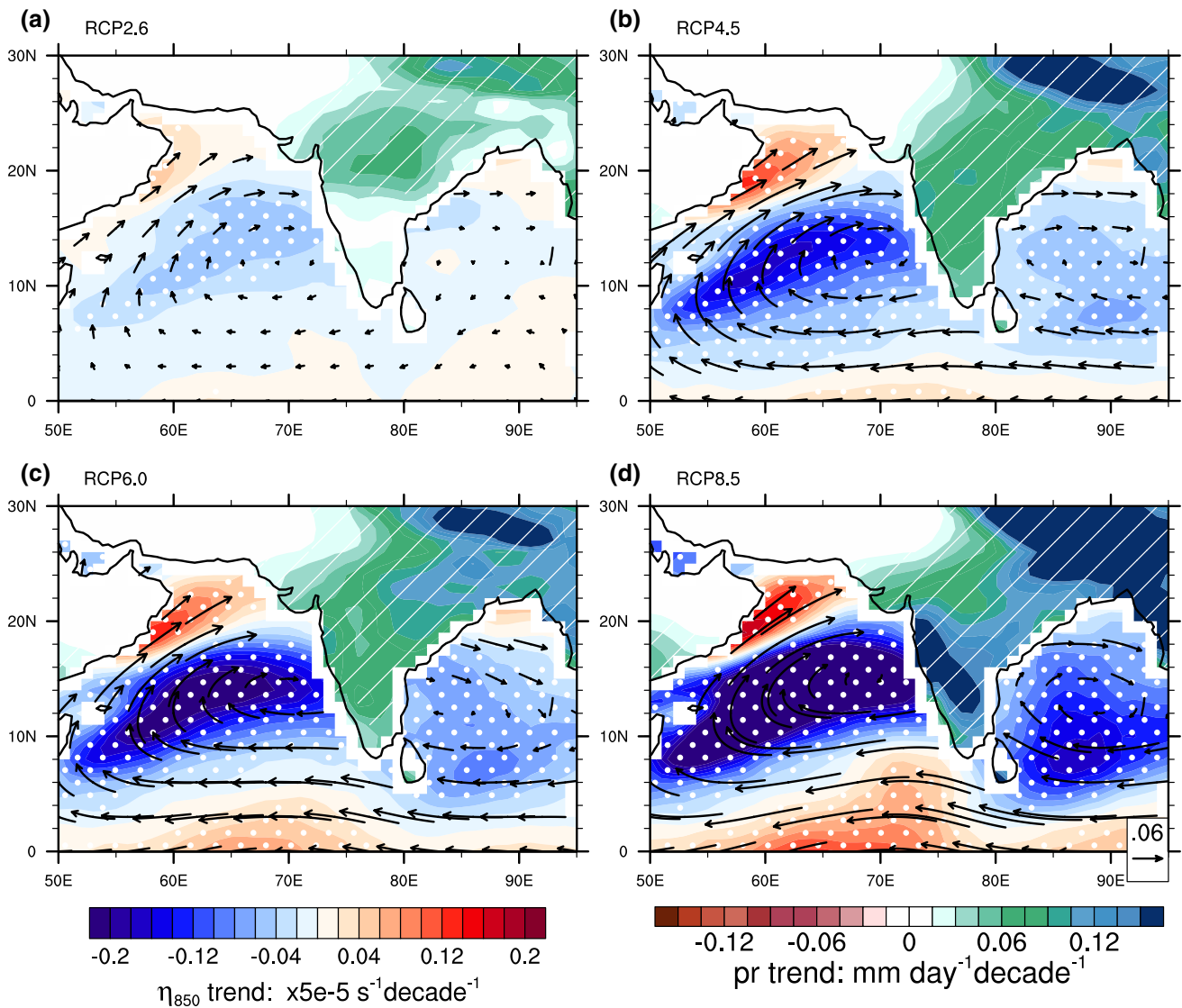


Fig. 3 Linear trends (2006–2099) in oceanic winds at 850 hPa (vectors; $\text{m s}^{-1} \text{ decade}^{-1}$), absolute vorticity (shading over oceans; $5 \times 10^{-5} \text{ s}^{-1} \text{ decade}^{-1}$) and land precipitation ($\text{mm day}^{-1} \text{ decade}^{-1}$)

for **a** RCP2.6, **b** RCP4.5, **c** RCP6.0, and **d** RCP8.5 scenarios respectively. Stippling show regions with statistically significant ($p < 0.05$) trends

of LLJ also experiences a poleward shift in a warming climate (Fig. 4c), similar to that of zero absolute vorticity over the Arabian Sea. The ensemble mean linear trends in $\Phi_{U_{\max}}$ for RCP4.5, RCP6.0, and RCP8.5 are statistically significant ($p < 0.05$), with values of 0.11, 0.12, and 0.17 degrees decade^{-1} respectively (Fig. 4d). The linear trends in $\Phi_{\eta=0'}$ and $\Phi_{U_{\max}}$ for future projections suggest that the degree of shift in the LLJ depends on the degree of radiative forcing. Under extreme warming scenario, the LLJ core would shift poleward from its climatological location by $\sim 1.5^\circ$ (based on $\Phi_{\eta=0}$) and $\sim 2^\circ$ (based on $\Phi_{U_{\max}}$). The trend in $\Phi_{\eta=0'}$ suggests that the LLJ shift seen in the observations and models has a strong connection to the underlying dynamics of the monsoon circulation.

It is worth investigating, whether the previous generation of climate models concurs with the CMIP5 simulations. Consistent, with CMIP5 results, CMIP3 ensembles also show a poleward shift the $\Phi_{\eta=0'}$ (Fig. 5). The stronger emission scenarios of SRESA1B and SRESA2 show statistically significant ($p < 0.05$) trends in $\Phi_{\eta=0'}$, with values of 0.11 and 0.12 degrees decade^{-1} respectively.

As mentioned in Sect. 1, several studies have noted that the whole monsoon circulation is shifting poleward in a warming scenario (Ashrit et al. 2003; May 2002; Menon et al. 2013b). To reassess this point in the context of LLJ shift in a quantitative manner, the annual anomalies in latitude at which the zonal mean (50°E–70°E) U850 turns

Fig. 4 **a** Time series of anomalies in the latitude (degrees) of zero absolute vorticity ($\Phi_{\eta=0}'$) over Arabian Sea, **b** box plot showing linear trends in latitudinal shift (degrees decade⁻¹) in $\Phi_{\eta=0}'$ for various CMIP5 experiments. **c, d** are same as (a) and (b) except for the LLJ core. The ensemble mean trends are represented by *asterisks* in (c) and (d). The LLJ core latitude is defined as the latitude of 850 hPa zonal wind maximum over the Arabian Sea (50°E–70°E, 5°N–25°N). Three year running mean is applied to all time series. Trends are statistically significant at 5 % level for RCP4.5, RCP6.0, and RCP8.5 experiments and for ERAI

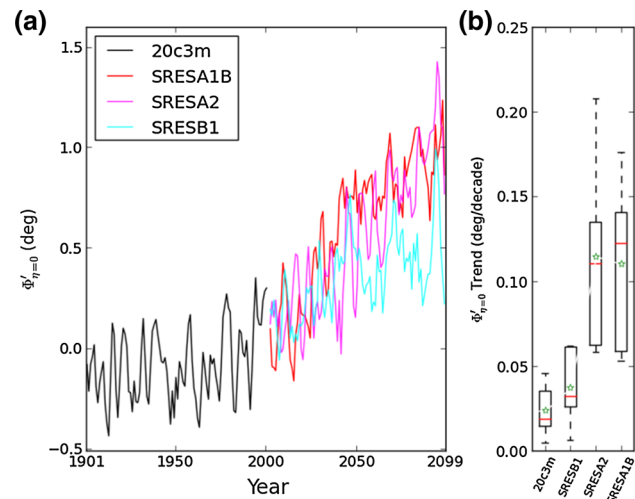
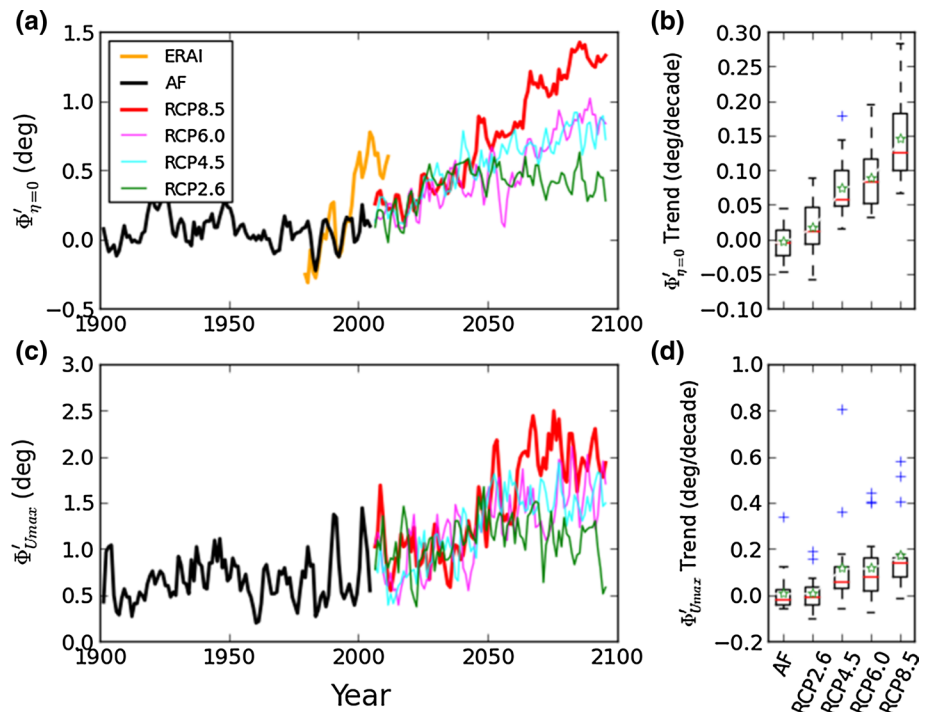


Fig. 5 **a, b** Same as Fig. 4a, b, except for CMIP3 experiments. Trends are statistically significant at 5 % level for SRESA1B and SRESA2

from easterly to westerly ($\Phi_{U850=0}'$) are calculated. Consistent with poleward shift in LLJ core and $\Phi_{\eta=0}'$, the latitude at which the easterlies change its direction to westerlies is also shifting northward indicating a poleward shift of the whole monsoon circulation (Fig. 6). The ensemble mean linear trends in $\Phi_{U850=0}'$ are found to be 0.05, 0.07, and 0.12 degrees decade⁻¹ for RCP4.5, RCP6.0, and RCP8.5 experiments. Similar to the trend in $\Phi_{\eta=0}'$, ERAI shows a linear trend of 0.3 degrees decade⁻¹ in $\Phi_{U850=0}'$ in the 34 years of analysis. The observed and simulated

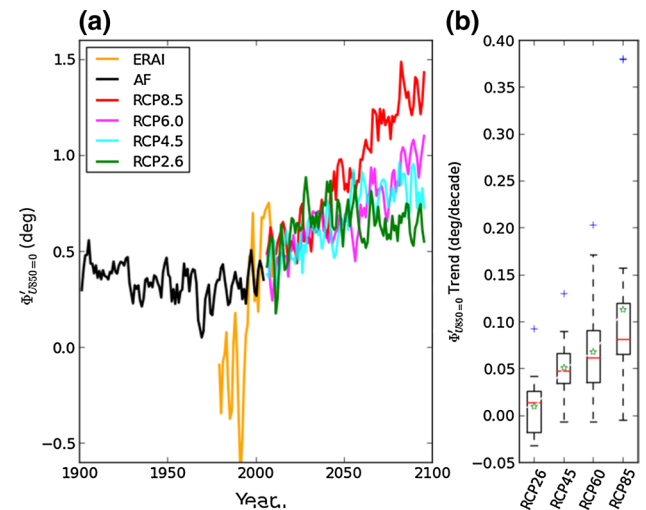
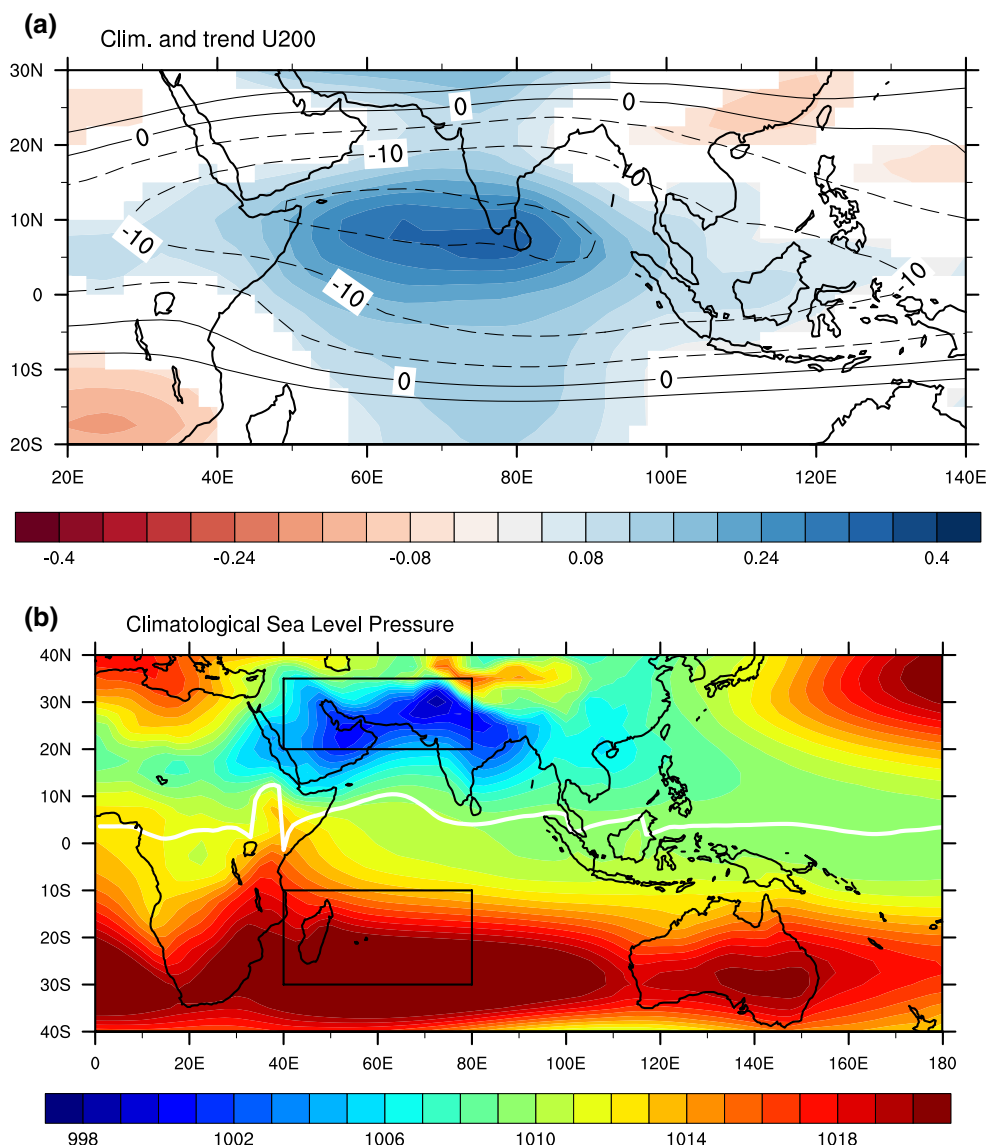


Fig. 6 **a, b** Same as Fig. 4a, b, except for anomalies in the latitudes at which zonal mean (50°E–70°E) zonal winds changes its direction from easterly to westerly ($\Phi_{U850=0}'$). Trends are statistically significant at 5 % level for RCP4.5, RCP6.0, and RCP8.5 experiments and for ERAI

changes in the monsoon low level flow can naturally pose questions about the possible changes in the upper level flow. The linear trends in upper-level winds (200 hPa) do not show any significant change in the mean position of the TEJ in the RCP8.5 simulations (Fig. 7a). However, we find a substantial weakening of the TEJ in the strongest future scenario, consistent with earlier studies (Abish et al. 2013).

Fig. 7 **a** JJAS climatology (1981–2000) of zonal winds at 200 hPa (contours; -15 to 5 m s^{-1} with interval of 5 m s^{-1}) and the RCP8.5 linear trend (2006–2099) in zonal winds at 200 hPa (shading; $\text{m s}^{-1} \text{ decade}^{-1}$); **b** JJAS climatology (1981–2000) of PSL (hPa). The white contour indicates the JJAS mean position of zero absolute vorticity. The two black boxes indicate the north and south regions selected for computing the PSL gradient and land-sea temperature contrast



4 Dynamics of poleward shift in LLJ

The monsoon south-westerlies are a response to the land-sea temperature contrast (ΔTS) between Southeast Asian land-mass and surrounding Indian Ocean (Webster and Fasullo 2003). The faster rate of heating of the land compared to ocean results in a stronger cross-equatorial pressure gradient (ΔPSL) over the Indian Ocean during summer and as a result $\eta = 0$ contour exhibits larger poleward intrusion over the Arabian Sea compared to other regions along the equator (Tomas and Webster 1997). During boreal summer, the strong heating over land mass creates a low pressure area over north-west India and adjoining region. The high pressure region over southern Indian Ocean and the heat low over land create a strong ΔPSL over Indian Ocean (Fig. 7b). The $\eta = 0$ contour over the Arabian Sea lies between 8 and 10° poleward of the equator (white line

in Fig. 7b), as illustrated by Tomas and Webster (1997). In a warming climate the ΔTS and subsequently ΔPSL could strengthen. In order to calculate ΔTS and ΔPSL over Arabian Sea where the LLJ core is located, we choose two boxes—one over north-west India and adjoining land mass and another over southern Indian Ocean, as indicated by the black boxes in Fig. 7b. The ΔTS (ΔPSL) is calculated as the difference of the area averaged surface temperature (PSL) between the northern and southern boxes.

Different definitions of land-sea temperature contrast can be seen in the literature (Fu and Fletcher 1985; Li and Yanai 1996; Sun et al. 2010; Wu et al. 2012). Most of them have considered the land region including Tibetan Plateau in their calculations of land-sea temperature contrast. Interestingly, Sun et al. (2010) claims that the relation between ISM strength and land-sea temperature contrast has weakened since 2000 in CMIP3 simulations, as a result of increased

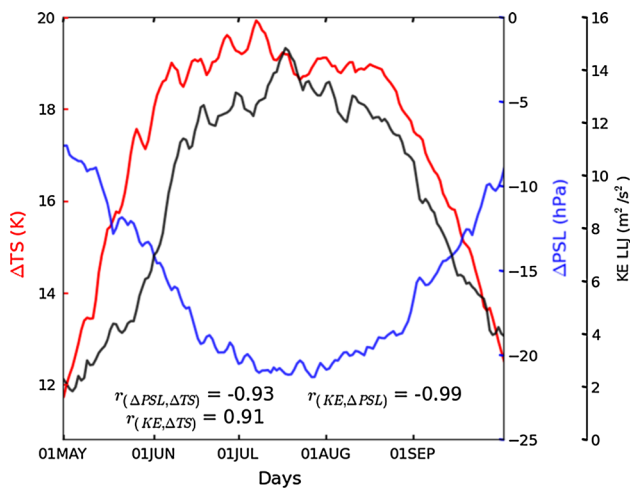


Fig. 8 Evolution of land-sea temperature contrast (K), cross-equatorial pressure gradient (hPa), and kinetic energy of low level Jet ($\text{m}^2 \text{s}^{-2}$) from 1st May to 30th September. ΔTS and ΔPSL are calculated as the difference of the respective parameters between the northern (20°N – 35°N and 40°E – 80°E) and southern (35°S – 10°S and 40°E – 80°E) boxes in Fig. 7b. Twenty year (1981–2000) daily climatology from ERAI is used for calculations. Cross-correlations between the variables are shown. The grid points over ocean in the northern box (in Fig. 7b) are masked while computing land-sea temperature contrast

tropical convection. As our main focus is LLJ, we propose a slightly different definition of land-sea temperature contrast, in conformity with the LLJ theory proposed by Tomas and Webster (1997). The northern (land) and southern (ocean) boxes considered (see Fig. 7b) here lies over heat induced low pressure region over North-West India & adjoining regions and high pressure region over southern Indian Ocean. In addition these regions cover the longitudinal extent of LLJ. In order to validate the assumption that ΔTS is driving ΔPSL and thereby LLJ, the evolutions of ΔTS , ΔPSL , and Kinetic Energy of LLJ (KELLJ) are examined in the observations. Fig. 8 shows the daily climatology of ΔTS , ΔPSL , and KELLJ between 1st May and 30th September. The strong correlation between ΔTS and ΔPSL ($r = -0.93$), ΔTS and KELLJ (0.91), and ΔPSL and KELLJ (-0.99) indicates the strong dynamical linkage between these parameters. Although the detailed mechanism of LLJ formation may not be elucidated from this simple analysis, the lead (~ 1 – 2 weeks) of ΔTS ahead of ΔPSL hints that former drives meridional pressure gradient and thereby LLJ. This gives credence to our argument that the LLJ dynamics has strong association with land-sea contrast.

The inter-annual variability of ΔTS and $\Phi_{\eta=0}'$ for historical AF and RCP8.5 ensembles is illustrated in Fig. 9a. Both ΔTS and $\Phi_{\eta=0}'$ shows an increasing trend in RCP8.5 experiments. The high correlation of 0.9 between the two parameters in the future projections suggests that intensification of ΔTS is the predominant driving mechanism for the poleward

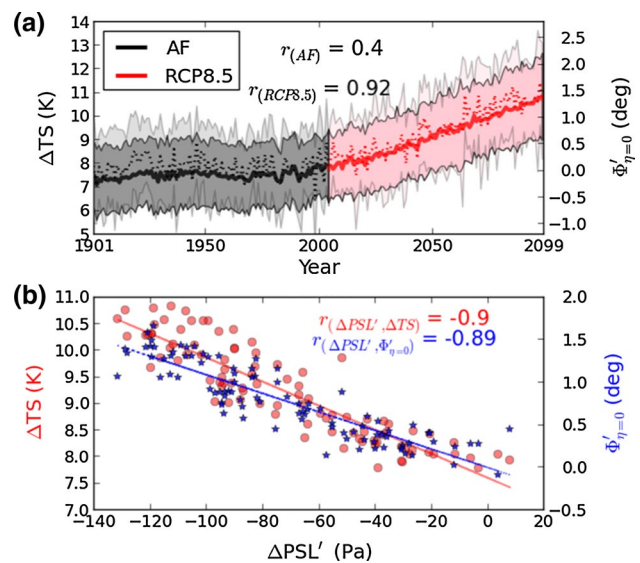


Fig. 9 **a** Inter-annual variability in land-sea temperature contrast (K; *bold line*) and the anomaly in mean latitudinal position of zero absolute vorticity (degrees; *broken line*). The data for this plot are constructed from historical AF simulations (1901–2005) and RCP8.5 simulations (2006–2099); **b** *scatter plot* showing the relationships between land-sea temperature contrasts and north–south PSL gradient and anomaly in the latitudinal position of zero absolute vorticity (RCP8.5). The *shading* in **a** shows ensemble spread. Correlations between the parameters are indicated. All correlation values are statistically significant ($p < 0.05$)

shift in LLJ. In the historical AF simulations the correlation between ΔTS and $\Phi_{\eta=0}'$ has a rather moderate value of 0.4 although it is statistically significant. The amplitudes of their interannual variability in the historical era are weak compared to the future projections. An alternate interpretation would be that ΔTS will gain more dominance in a warming scenario and hence can drive changes in meridional pressure gradient and LLJ. Further, the relation between ΔPSL versus ΔTS and ΔPSL versus $\Phi_{\eta=0}'$ are examined (Fig. 9b). The close association of ΔPSL versus ΔTS ($r = -0.9$) and ΔPSL versus $\Phi_{\eta=0}'$ (-0.89), strongly suggests the role of intensified land-sea contrast and thereby intensified cross-equatorial pressure gradient in inducing a latitudinal shift in the LLJ. In order to obtain a broader understanding of changes in pressure gradient, the linear trends in PSL for RCP8.5 ensemble mean is calculated during 2006–2099 (Fig. 10). The trend pattern shows a tropics-wide increase in PSL and decrease over extra tropics. The zonal mean trends show a strong PSL gradient directed towards northern hemisphere. The large-scale PSL drop over Middle East and North African desert regions and increase over Indian land region are also noteworthy. The strong decrease in PSL over desert regions north-west of India favors a poleward shift in monsoon low level winds.

The ISM low level circulation is the driver of cross-equatorial oceanic heat transport (H_{η}) over the Northern Indian

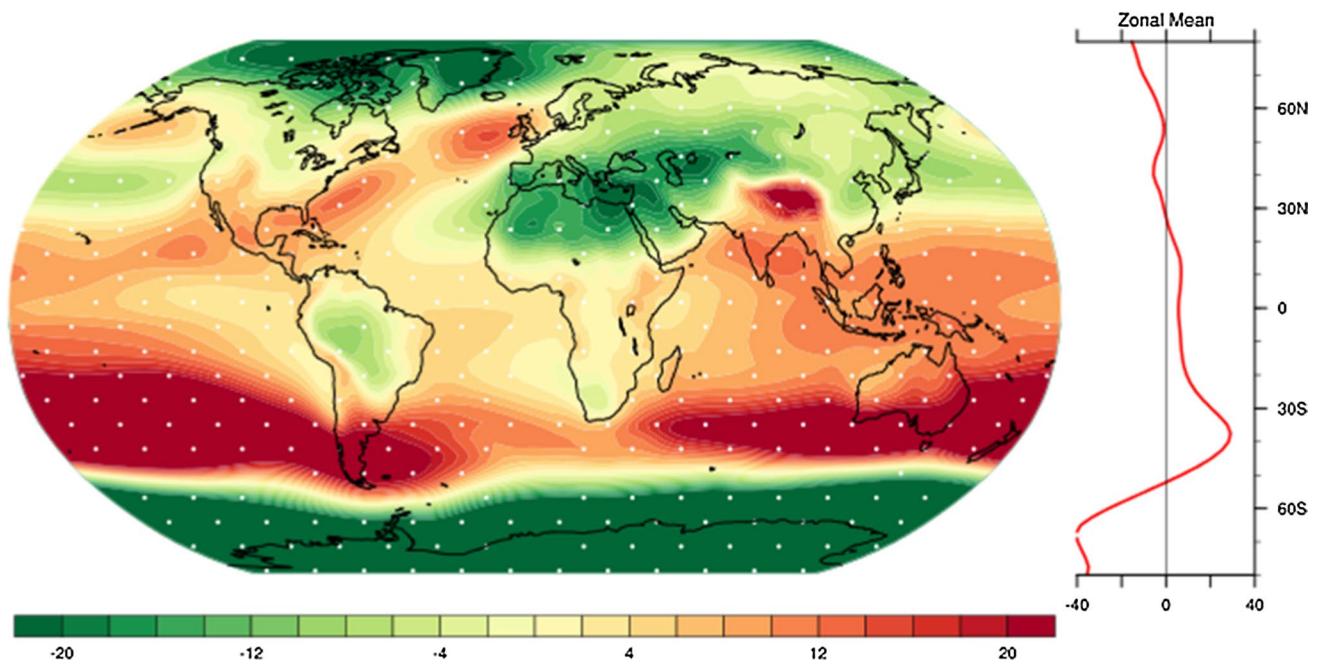


Fig. 10 Linear trend (2006–2099) in Sea level pressure (Pa decade^{-1}) in RCP8.5 ensemble mean. Zonal mean of Sea level pressure trends are shown on *right panel*. Stippling shows statistically significant ($p < 0.05$) trends

Ocean. The cross-equatorial heat transport over the Indian Ocean is critical for the regulation of ISM interannual variability and annual cycle by homogenizing SST between southern and northern Indian Ocean (Webster and Fasullo 2003). Further, we investigate the changes in H_y over the Arabian Sea, where LLJ shift is dominant. Consistent with the theoretical expectations, cross-equatorial oceanic heat transport over the Arabian Sea during JJAS is found to be declining at a rate of $-5.8 \times 10^{11} \text{ W decade}^{-1}$ ($p < 0.05$), in RCP8.5 scenario (Fig. 11). This suggests that the ocean–atmosphere coupling over the ISM region could be affected by the changes in the LLJ. Further investigation is needed to find the ocean feedback effects due to the changes in LLJ strength and position, which is beyond the scope of present study.

To conclude, the dynamics of poleward shift in monsoon LLJ can be summarized with the help of a schematic (Fig. 12) as follows:

1. The land surface experiences a faster rate of heating compared to the Oceans, as the atmosphere warms under the influence of enhanced GHGs.
2. The faster rate of heating over land results in a deepening of the low pressure area over land and subsequently strengthens the cross-equatorial pressure gradient.
3. The stronger cross-equatorial pressure gradient pushes the low-level circulation and zero absolute vorticity contour further north. The evolution of ΔTS , ΔPSL , and KELLJ in the reanalysis (Fig. 8) also supports this mechanism. Poleward shift in $\eta = 0$ will result

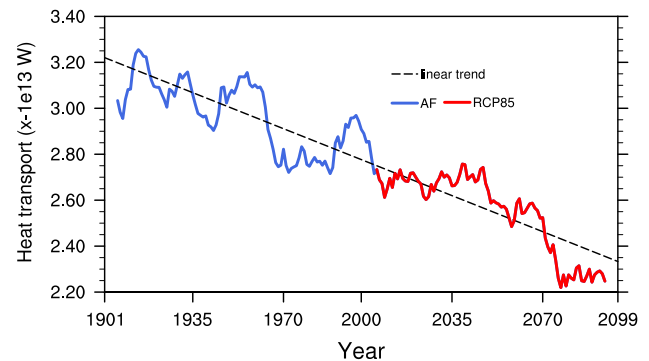


Fig. 11 Time series of area averaged meridional heat transport ($-1 \times 10^{13} \text{ W}$) during JJAS season over Arabian Sea (40°E – 75°E ; EQ – 25°N) for historical AF (1901–2005; *blue line*) and RCP8.5 (2006–2099; *red line*). Decadal smoothing is applied to the time series

in enhanced (decreased) area of divergence (convergence) north of equator. This mechanism suggests that the observed poleward shift of LLJ and the associated changes in the precipitation pattern over the west coast of India might be caused by the global warming.

5 Systematic biases

In this section, we deliberate the systematic biases in the CMIP5 simulation that influences the present results and

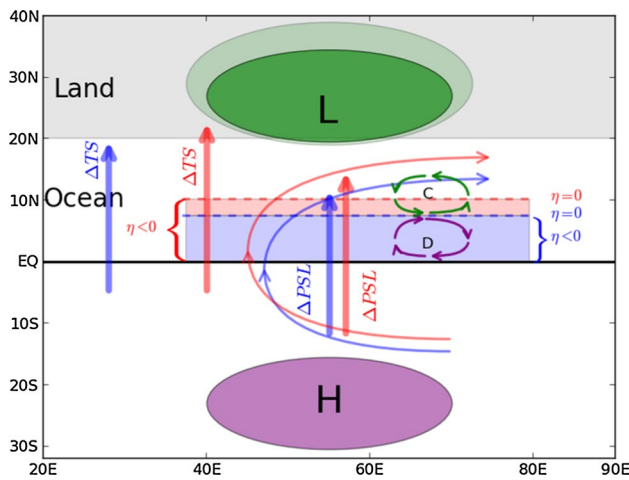


Fig. 12 Schematic diagram showing the dynamics of poleward shift in LLJ in a warming climate. Blue (red) curves illustrate the monsoon low level circulation in current (warm) climate. Blue (red) bold arrows indicate the strength and direction of cross-equatorial pressure gradient and land-sea temperature contrast in current (warm) climate. Blue (red) dashed line indicates the location of zero absolute vorticity contour in current (warm) climate. The green (purple) ellipse indicates the low (high) pressure area. The thermal expansion of low pressure area over land, in a warmer climate is indicated by light green ellipse that envelope the green ellipse. The concept of LLJ as convergence (C)-divergence (D) couplet about $\eta = 0$ contour is also illustrated

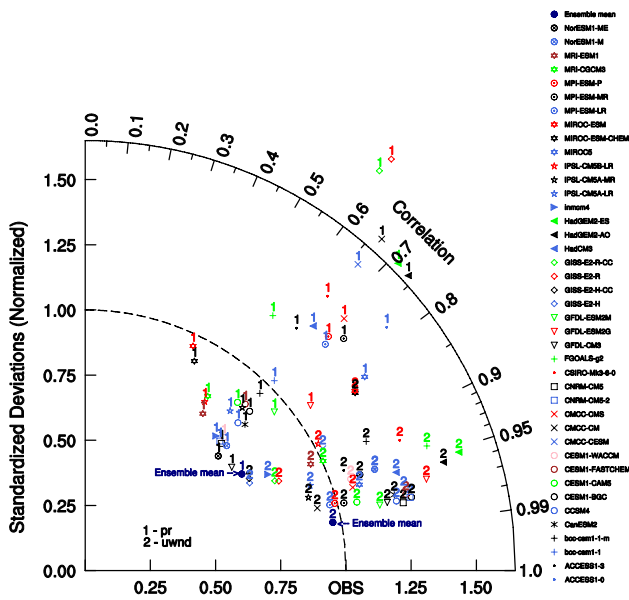


Fig. 13 Taylor diagram for model simulated JJAS mean precipitation and zonal winds at 850 hPa. The individual model simulated 1979–2005 climatology of JJAS mean precipitation and zonal winds area averaged over ISM domain (40°E–120°E, 10°S–30°N) are compared with observations. The precipitation observations are taken from GPCP and winds from the ERAI reanalysis

its implications. It is important to examine whether the present results are affected by the systematic biases. Another issue is the fidelity of the CGCMs in simulating winds and precipitation. As mentioned earlier, no single CGCM can simulate all features of ISM realistically (Sperber et al. 2013). The skill of ensemble mean outperforms individual models probably due to cancellation of errors (Kharin et al. 2001). In the analyses presented so far, we have used a subset of CMIP5 CGCMs that have the required data for historical AF and all RCP experiments. Before drawing broad conclusions, it needs to be investigated that whether the robustness of the results is affected by the ensemble sample sizes. The Taylor diagram of zonal winds and precipitation (Fig. 13) agrees with Sperber et al. (2013) that the ensemble mean has stronger skill than individual models, especially for zonal winds. In the case of precipitation, the ensemble mean has larger spatial correlation compared to individual models, but with weaker amplitude of spatial variability than many individual CGCMs. Further, the simulation of low-level winds has less spread compared to precipitation and the ensemble mean of low-level winds shows very high skill ($r = 0.98$; $r = 0.85$ for precipitation).

One of most highlighted systematic errors in the CMIP5 simulation of monsoon is the bias in SST seen in the Arabian Sea during pre-monsoon season (Levine et al. 2013; Marathayil et al. 2013). We first investigate if the cold bias in Arabian Sea SST has any impact on the trend in Φ_{U850} . The scatter plot between northern Arabian Sea SST bias and Φ_{U850} trend for RCP8.5 (Fig. 14) shows that virtually no relation exists between the two. The bias in SST does not seem to affect the shift in LLJ core in these simulations. Similar results were obtained for $\Phi_{\eta=0}$ (figure not shown). Also the trends in other RCP scenarios are not affected by the cold SST bias in the Arabian Sea.

To assess the effect of interpolation of data on a common $1^\circ \times 1^\circ$ grid, the calculations of Φ_{U850} and $\Phi_{\eta=0}$ are repeated on model's native grids. The mean value of Φ_{U850} in RCP8.5 experiment is found to be 12.31°N (12.17°N) with a standard deviation of 1.47 (1.53) for native (interpolated) GFDL-ESM2 M, which is a coarse resolution model ($2^\circ \times 2.5^\circ$). Identical results are obtained for $\Phi_{\eta=0}$ as well, with a mean value of $11.05 \pm 0.77^\circ\text{N}$ ($11.17 \pm 0.82^\circ\text{N}$) on native (interpolated) grids. The same calculations for CCSM4, which is a high resolution ($0.9^\circ \times 1.25^\circ$) model, yielded a mean value of $12.36 \pm 1.78^\circ\text{N}$ ($12.31 \pm 1.79^\circ\text{N}$) on native (interpolated) grid for Φ_{U850} . The mean position of $\Phi_{\eta=0}$ is found to be located at $12.0 \pm 0.93^\circ\text{N}$ ($11.93 \pm 0.93^\circ\text{N}$) in CCSM4 native (interpolated) grids. Similar results are obtained for other models as well, which are not elaborated here for the sake of brevity. This analysis shows that the interpolation of winds to a common grid

Fig. 14 Scatter plot of Northern Arabian Sea (15°N – 25°N , 50°E – 70°E) SST bias (K) and RCP8.5 linear trend (2006–2099) in the JJAS mean latitudinal position (degrees) of LLJ core, as defined by the maxima of 850 hPa zonal wind (over 5°N – 25°N and 50°E – 70°E), for CMIP5 models. Regression line is shown. MAM climatology (1981–2000) is used to calculate SST bias

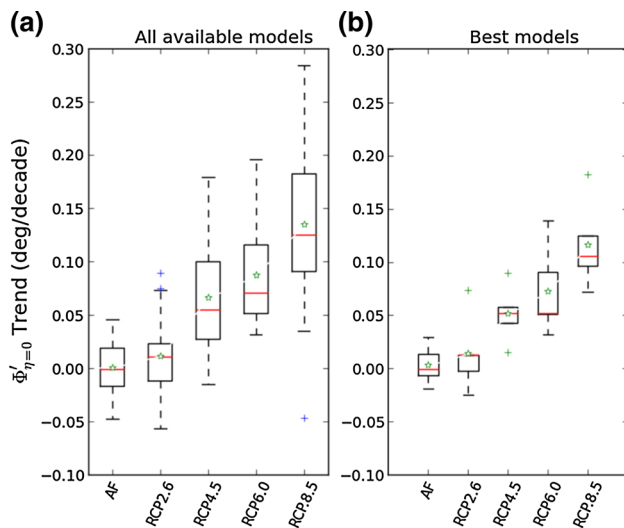
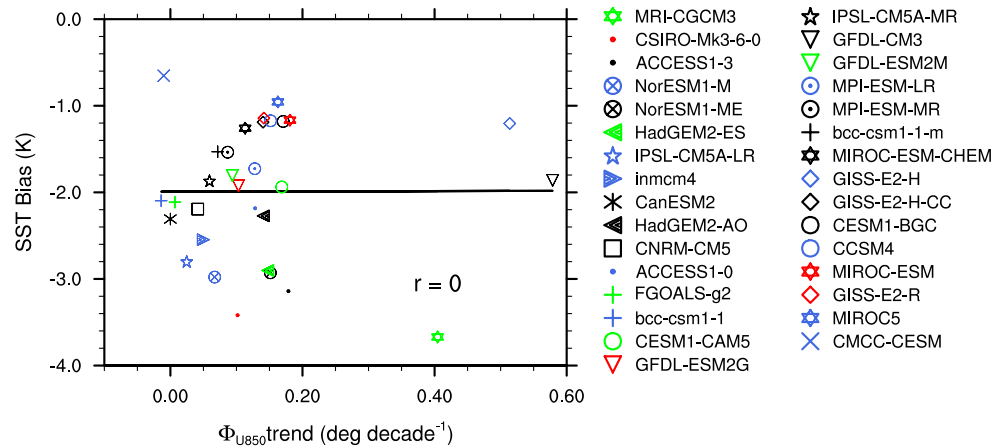


Fig. 15 Box plots showing trends in latitudinal position of zero absolute vorticity for **a** all available ensembles for each of the experiments and **b** the best five models for ISM precipitation that are selected based on the Taylor diagram in Fig. 13

introduced only negligible errors in the calculations of Φ_{U850} and $\Phi_{\eta=0}$.

To understand the uncertainty in trends of $\Phi_{\eta=0}'$ due to ensemble sample sizes, we calculated the linear trends in $\Phi_{\eta=0}'$ for all available models for each experiment (Fig. 15a), which yields identical results to that obtained with the subset of CGCMs which are common across all experiments. We repeated the same analysis with five ‘best’ models (based on Taylor diagram in Fig. 13 for the mean JJAS precipitation), yielding similar results (Fig. 15b), but with slightly weaker trends. Comparison of Fig. 15a with Fig. 4b, suggests that different ensemble sample sizes do not alter the trend and further strengthens our confidence in the poleward shift in monsoon LLJ in a warming climate reported from the analysis of CMIP5 simulations.

6 Summary and discussion

The land-sea temperature contrast over Indian monsoon region will amplify in a global warming scenario. The ISM low level circulation, especially the LLJ is found to shift poleward in response to the increased land-sea contrast. The poleward shift in LLJ is accompanied by a corresponding shift in the latitude of zero absolute vorticity over the Arabian Sea. The magnitude of the poleward shift in LLJ is found to be proportional to the degree of radiative forcing. As a consequence of the poleward shift, the LLJ seems to be strengthening (weakening) north (south) of 15°N over the Arabian Sea. Within the framework of CMIP5 experiments, the Indian land region would experience a wet trend in a warmer climate. The ERAI reanalysis data show a poleward shift in LLJ in the last three decades. The observed precipitation pattern on the Western Ghats and adjoining regions of India shows a wet (dry) pattern in the north (south), consistent with the shift in LLJ in the reanalysis. The ensemble mean of CMIP5 simulations in the historical AF experiment also shows a poleward shift in the LLJ in the last three decades of the simulation. However, the centennial trends in the historical AF ensemble do not show a statistically significant shift in LLJ location. This is not surprising, as the effects of the global warming on northern hemispheric hydrological cycle started emerging since 1980s (Wu et al. 2013). The robustness of the results is verified by ensuring that the SST bias, interpolation of the data, and ensemble sample sizes have negligible effects on the linear trends in LLJ latitudinal position.

In this study, we have presented evidences of a poleward shift in monsoon LLJ in both observations as well as in future scenario simulations using CGCMs. The poleward shift in LLJ is consistent with the widening of tropics (Fu 2006; Seidel and Randel 2007) and poleward shifts in sub-tropical jetstream and mid-latitude storm tracks (IPCC 2007; Fu and Lin 2011). The observed precipitation pattern over the Western Ghats shows a strong response to

the shift in LLJ, with a wet (dry) trend over north (south) of about 16°N. Recent studies that addressed this issue suggested a weakening of ISM circulation as a result of increased atmospheric stability due to global warming (Krishnan et al. 2013; Rajendran et al. 2012). However, the ISM weakening theory is not consistent with the observed increase in precipitation north of 16°N. Moreover, this theory also fails to explain the reason for increased stability only over south of 16°N. We suspect that the increased stability over southern part of the Arabian Sea seen in the analysis of Rajendran et al. (2012) could be partly a result of the poleward shift in the monsoon LLJ. The LLJ can be viewed as a convergence-divergence couplet about $\eta = 0$ contour, with the convergence zone lying north of $\eta = 0$ (Tomas and Webster 1997). As the $\eta = 0$ contour shift northward, the divergence zone between equator and $\eta = 0$ will expand and the result could be an increased stability over that region. This mechanism can very well explain the decreased (increased) precipitation over northern (southern) Western Ghats in the observations. The trends in orographic precipitation pattern in future simulations needs to be interpreted with care. High resolution simulations have already shown a wet (dry) precipitation trends over west coast of India north (south) of 16°N (Rajendran et al. 2013). Our analysis using coarse resolution CGCM simulations could not bring out the fine-scale features of regional precipitation changes. However, the poleward shift in monsoon LLJ is robust in CGCM simulations and reanalysis. Part of the weakening in LLJ could be compensated by the increased moisture influx in a warming environment and this may prevent a stronger decrease in precipitation south of 16°N. At the same time, the north-western India has a strong possibility of getting increased precipitation due to the dual effects of poleward shift in LLJ and enhanced moisture content of the air in a warming scenario. The spatial structure of TEJ weakening is different compared to LLJ, as the former does not show any latitudinal shift. One of the reasons of the TEJ weakening could be the weakening of the upper level meridional temperature gradient as suggested by Abish et al. (2013) which possibly explains the spatially coherent weakening of TEJ. Further investigation is needed to clearly understand the role of static stability versus land–ocean temperature contrast in deciding the fate of ISM circulation in a warming climate.

Our results have important societal implications in the wake of concerns over the preservation of ecologically fragile Western Ghats region (Gadgil et al. 2011; Kasturirangan et al. 2013). The decreased precipitation over the southern regions of the Western Ghats could lead to a water stress in those places. In the northern regions, possibilities of heavy precipitation events are high, in the wake of increased wind speeds and higher moisture content of the air in a warmer

climate. The South Asia is already identified as a region with high flood risk under projected warming scenarios (Hirabayashi et al. 2013). In the wake of the limitations of coarse resolution climate models, further investigations with high resolution models needs to be undertaken to quantify the potential climate change risks over regions like Western Ghats. Also, our results suggest oceanic impact of the changes in LLJ. The decline in the oceanic heat transport could potentially affect the ISM interannual variability. The poleward shift in LLJ can potentially cool the SSTs over the northern Arabian Sea, which in turn can affect the intraseasonal variability of ISM as well. Thus the changes in ocean–atmosphere coupling over the Indian Ocean due to projected changes in LLJ strength and position needs a thorough investigation in order to obtain a complete picture of the impact of global warming on Indian Summer Monsoon.

Acknowledgments The Center for Prototype Climate Modeling (CPCM) is fully funded by the Government of Abu Dhabi through New York University Abu Dhabi Research Institute grant. The authors thank various modeling groups that provided CGCM simulations of CMIP3 and CMIP5 experiments. NYUAD HPC resources are utilized for this work.

References

- Abish B, Joseph PV, Johannessen OM (2013) Weakening trend of the tropical easterly jet stream of the boreal summer monsoon season 1950–2009. *J Clim* 26(23):9408–9414. doi:10.1175/jcli-d-13-00440.1
- Ajayamohan RS, Rao SA (2008) Indian ocean dipole modulates the number of extreme rainfall events over India in a warming environment. *J Meteorol Soc Jpn* 86:245–252
- Ajayamohan RS, Merryfield WJ, Khari VV (2010) Increasing trend of synoptic activity and its relationship with extreme rain events over central India. *J Clim* 23(4):1004–1013
- Ashrit RG, Douville H, Kumar KR (2003) Response of the Indian monsoon and ENSO–monsoon teleconnection to enhanced greenhouse effect in the CNRM coupled model. *J Meteorol Soc Jpn* 81(4):779–803
- Ashrit RG, Kitoh A, Yukimoto S (2005) Transient response of ENSO–monsoon teleconnection in MRI CGCM. 2 climate change simulations. *J Meteorol Soc Jpn* 83:273–291
- Bollasina M, Ming Y, Ramaswamy V (2011) Anthropogenic aerosols and the weakening of the South Asian summer monsoon. *Science* 334(6055):502–505. doi:10.1126/science.1204994
- Dee DP, Uppala SM, Simmons AJ, Berrisford P, Poli P, Kobayashi S, Andrae U, Balmaseda MA, Balsamo G, Bauer P, Bechtold P, Beljaars ACM, van de Berg L, Bidlot J, Bormann N, Delsol C, Dragani R, Fuentes M, Geer AJ, Haimberger L, Healy SB, Hersbach H, Hólm EV, Isaksen L, Kållberg P, Köhler M, Matricardi M, McNally AP, Monge-Sanz BM, Morcrette JJ, Park BK, Peubey C, de Rosnay P, Tavolato C, Thépaut JN, Vitart F (2011) The ERA-interim reanalysis: configuration and performance of the data assimilation system. *Q J R Meteorol Soc* 137(656):553–597. doi:10.1002/qj.828
- Findlater J (1969) A major low-level air current near the Indian ocean during the northern summer. *Q J R Meteorol Soc* 95(404):362–380. doi:10.1002/qj.49709540409

- Fu Q (2006) Enhanced mid-latitude tropospheric warming in satellite measurements. *Science* 312. doi:[10.1126/science.1125566](https://doi.org/10.1126/science.1125566)
- Fu C, Fletcher JO (1985) The relationship between tibet-tropical ocean thermal contrast and interannual variability of Indian monsoon rainfall. *J Clim Appl Meteorol* 24(8):841–847. doi:[10.1175/1520-0450\(1985\)024<0841:TRBTTO>2.0.CO;2](https://doi.org/10.1175/1520-0450(1985)024<0841:TRBTTO>2.0.CO;2)
- Fu Q, Lin P (2011) Poleward shift of subtropical jets inferred from satellite-observed lower-stratospheric temperatures. *J Clim* 24(21):5597–5603. doi:[10.1175/JCLI-D-11-00027.1](https://doi.org/10.1175/JCLI-D-11-00027.1)
- Gadgil S, Gadgil S (2006) The Indian monsoon, GDP and agriculture. *Econ Polit Wkly* 41(47):4887–4895
- Gadgil M, Krishnan BJ, Ganeshaiah KN, Vijayan VS, Borges R, Sukumar R, Noronha L, Nayak SV, Subramaniam DK, Varma RV, Gautam SP, Navalgund RR, Subrahmanyam GV (2011) Report of the Western Ghats ecology expert panel part 1. New Delhi
- Goswami BN, Venugopal V, Sengupta D, Madhusoodanan MS, Xavier PK (2006) Increasing trend of extreme rain events over India in a warming environment. *Science* 314(5804):1442–1445. doi:[10.1126/science.1132027](https://doi.org/10.1126/science.1132027)
- Guhathakurta P, Rajeevan M (2008) Trends in the rainfall pattern over India. *Int J Climatol* 28(11):1453–1469. doi:[10.1002/joc.1640](https://doi.org/10.1002/joc.1640)
- Hirabayashi Y, Mahendran R, Koirala S, Konoshima L, Yamazaki D, Watanabe S, Kim H, Kanae S (2013) Global flood risk under climate change. *Nat Clim Change* 3(9):816–821. doi:[10.1038/nclim.2013.191](https://doi.org/10.1038/nclim.2013.191)
- IPCC (2007) Contribution of working group I to the fourth assessment report of the intergovernmental panel on climate change, 2007. Climate change 2007: the physical science basis. IPCC, Cambridge, UK and New York, USA
- Joseph PV, Raman PL (1966) Existence of low level westerly jet-stream over peninsular India during July. *Indian J Meteorol Geophys* 17:407–410
- Joseph PV, Sijikumar S (2004) Intraseasonal variability of the low-level jet stream of the Asian summer monsoon. *J Clim* 17(7):1449–1458. doi:[10.1175/1520-0442\(2004\)017<1449:IVO TLJ>2.0.CO;2](https://doi.org/10.1175/1520-0442(2004)017<1449:IVO TLJ>2.0.CO;2)
- Joseph PV, Simon A (2005) Weakening trend of the southwest monsoon current through peninsular India from 1950 to the present. *Curr Sci* 89(4):687–694
- Kasturirangan K, Babu CR, Mauskar JM, Chopra K, Kishwan J, Shanar D, Narain S, Roy PS, Tyagi A, Chandrasekharan I (2013) Report of the high level working group on Western Ghats, vol 1. New Delhi
- Kharin VV, Zwiers FW, Gagnon N (2001) Skill of seasonal hindcasts as a function of the ensemble size. *Clim Dyn* 17(11):835–843. doi:[10.1007/s003820100149](https://doi.org/10.1007/s003820100149)
- Kitoh A, Hirokazu E, Kumar KK, Iracema FAC, Prashant G, Tianjun Z (2013) Monsoons in a changing world: a regional perspective in a global context. *J Geophys Res Atmos* 118. doi:[10.1002/jgrd.50258](https://doi.org/10.1002/jgrd.50258)
- Krishnan R, Sabin TP, Ayantika DC, Kitoh A, Sugi M, Murakami H, Turner AG, Slingo JM, Rajendran K (2013) Will the South Asian monsoon overturning circulation stabilize any further? *Clim Dyn* 40(1–2):187–211. doi:[10.1007/s00382-012-1317-0](https://doi.org/10.1007/s00382-012-1317-0)
- Kumar KK, Kamala K, Rajagopalan B, Hoerling M, Eischeid J, Patwardhan SK, Srinivasan G, Goswami BN, Nemani R (2011) The once and future pulse of Indian monsoonal climate. *Clim Dyn* 36(11–12):2159–2170. doi:[10.1007/s00382-010-0974-0](https://doi.org/10.1007/s00382-010-0974-0)
- Lau KM, Kim KM (2006) Observational relationships between aerosol and Asian monsoon rainfall, and circulation. *Geophys Res Lett* 33. doi:[10.1029/2006GL027546](https://doi.org/10.1029/2006GL027546)
- Levine RC, Turner AG, Marathayil D, Martin GM (2013) The role of northern Arabian Sea surface temperature biases in CMIP5 model simulations and future projections of Indian summer monsoon rainfall. *Clim Dyn* 41(1):155–172. doi:[10.1007/s00382-012-1656-x](https://doi.org/10.1007/s00382-012-1656-x)
- Li C, Yanai M (1996) The onset and interannual variability of the Asian summer monsoon in relation to land-sea thermal contrast. *J Clim* 9(2):358–375. doi:[10.1175/1520-0442\(1996\)009<0358:TOAIVO>2.0.CO;2](https://doi.org/10.1175/1520-0442(1996)009<0358:TOAIVO>2.0.CO;2)
- Marathayil D, Turner AG, Shaffrey LC, Levine RC (2013) Systematic winter sea-surface temperature biases in the northern Arabian Sea in HiGEM and the CMIP3 models. *Environ Res Lett* 8(1):014028. doi:[10.1088/1748-9326/8/1/014028](https://doi.org/10.1088/1748-9326/8/1/014028)
- May W (2002) Simulated changes of the Indian summer monsoon under enhanced greenhouse gas conditions in a global time-slice experiment. *Geophys Res Lett* 29. doi:[10.1029/2001GL013808](https://doi.org/10.1029/2001GL013808)
- Meehl GA, Arblaster JM (2003) Mechanisms for projected future changes in south Asian monsoon precipitation. *Clim Dyn* 21(7–8):659–675. doi:[10.1007/s00382-003-0343-3](https://doi.org/10.1007/s00382-003-0343-3)
- Meehl GA, Covey C, Taylor KE, Delworth T, Stouffer RJ, Latif M, McAvaney B, Mitchell JFB (2007) THE WCRP CMIP3 multimodel dataset: a new era in climate change research. *Bull Am Meteorol Soc* 88(9):1383–1394. doi:[10.1175/BAMS-88-9-1383](https://doi.org/10.1175/BAMS-88-9-1383)
- Menon A, Levermann A, Schewe J (2013a) Enhanced future variability during India's rainy season. *Geophys Res Lett* 40(12):3242–3247. doi:[10.1002/grl.50583](https://doi.org/10.1002/grl.50583)
- Menon A, Levermann A, Schewe J, Lehmann J, Frieler K (2013b) Consistent increase in Indian monsoon rainfall and its variability across CMIP-5 models. *Earth Syst Dyn* 4(2):287–300. doi:[10.5194/esd-4-287-2013](https://doi.org/10.5194/esd-4-287-2013)
- Moss RH, Edmonds JA, Hibbard KA, Manning MR, Rose SK, van Vuuren DP, Carter TR, Emori S, Kainuma M, Kram T, Meehl GA, Mitchell JFB, Nakicenovic N, Riahi K, Smith SJ, Stouffer RJ, Thomson AM, Weyant JP, Wilbanks TJ (2010) The next generation of scenarios for climate change research and assessment. *Nature* 463(7282):747–756. doi:[10.1038/nature08823](https://doi.org/10.1038/nature08823)
- Nakicenovic N, Alcamo J, Davis G, de Vries B, Fenhann J, Gaffin S, Gregory K, Grübler A, Jung TY, Kram T, La Rovere EL, Michaelis L, Mori S, Morita T, Pepper W, Pitcher H, Price L, Riahi K, Roehrl A, Rogner H–H, Sankovski A, Schlesinger M, Shukla P, Smith S, Swart R, van Rooijen S, Victor N, Dadi Z (2000) Special report on emission scenarios. IPCC, UK
- Nigam S, Bollasina M (2010) “Elevated heat pump” hypothesis for the aerosol-monsoon hydroclimate link: “Grounded” in observations? *J Geophys Res Atmos* 115. doi:[10.1029/2009jd013800](https://doi.org/10.1029/2009jd013800)
- Rajendran K, Kitoh A, Srinivasan J, Mizuta R, Krishnan R (2012) Monsoon circulation interaction with Western Ghats orography under changing climate. *Theoret Appl Climatol* 110(4):555–571. doi:[10.1007/s00704-012-0690-2](https://doi.org/10.1007/s00704-012-0690-2)
- Rajendran K, Sajani S, Jayasankar CB, Kitoh A (2013) How dependent is climate change projection of Indian summer monsoon rainfall and extreme events on model resolution? *Curr Sci* 104(10):1409–1418
- Ramanathan V, Chung C, Kim D, Bettge T, Buja L, Kiehl JT, Washington WM, Fu Q, Sikka DR, Wild M (2005) Atmospheric brown clouds: impacts on South Asian climate and hydrological cycle. *Proc Natl Acad Sci USA* 102(15):5326–5333. doi:[10.1073/pnas.0500656102](https://doi.org/10.1073/pnas.0500656102)
- Seidel DJ, Randel W, J. (2007) Recent widening of the tropical belt: Evidence from tropopause observations. *J Geophys Res* 112. doi:[10.1029/2007JD008861](https://doi.org/10.1029/2007JD008861)
- Rayner NA, Parker DE, Horton EB, Folland CK, Alexander LV, Rowell DP, Kent EC, Kaplan A (2003) Global analyses of sea surface temperature, sea ice, and night marine air temperature since the late nineteenth century. *J Geophys Res* 108(D14):4407. doi:[10.1029/2002jd002670](https://doi.org/10.1029/2002jd002670)
- Sathiyamoorthy V (2005) Large scale reduction in the size of the tropical easterly jet. *Geophys Res Lett* 32(14). doi:[10.1029/2005gl022956](https://doi.org/10.1029/2005gl022956)
- Sperber KR, Annamalai H, Kang IS, Kitoh A, Moise A, Turner A, Wang B, Zhou T (2013) The Asian summer monsoon: an

- intercomparison of CMIP5 vs. CMIP3 simulations of the late 20th century. *Clim Dyn* 41(9–10):2711–2744. doi:[10.1007/s00382-012-1607-6](https://doi.org/10.1007/s00382-012-1607-6)
- Stowasser M, Annamalai H, Hafner J (2009) Response of the South Asian summer monsoon to global warming: mean and synoptic systems. *J Clim* 22(4):1014–1036. doi:[10.1175/2008jcli2218.1](https://doi.org/10.1175/2008jcli2218.1)
- Sun Y, Ding Y, Dai A (2010) Changing links between South Asian summer monsoon circulation and tropospheric land-sea thermal contrasts under a warming scenario. *Geophys Res Lett* 37(2). doi:[10.1029/2009gl041662](https://doi.org/10.1029/2009gl041662)
- Taylor KE, Stouffer RJ, Meehl GA (2011) An overview of CMIP5 and the experiment design. *Bull Am Meteorol Soc* 93(4):485–498. doi:[10.1175/BAMS-D-11-00094.1](https://doi.org/10.1175/BAMS-D-11-00094.1)
- Tokinaga H, Xie S-P (2011) Wave-and anemometer-based sea surface wind (WASWind) for climate change analysis. *J Clim* 24(1):267–285. doi:[10.1175/2010JCLI3789.1](https://doi.org/10.1175/2010JCLI3789.1)
- Tomas RA, Webster PJ (1997) The role of inertial instability in determining the location and strength of near-equatorial convection. *Q J R Meteorol Soc* 123(542):1445–1482. doi:[10.1002/qj.49712354202](https://doi.org/10.1002/qj.49712354202)
- Turner AG, Annamalai H (2012) Climate change and the South Asian summer monsoon. *Nat Clim Change* 2(8):587–595. doi:[10.1038/nclimate1495](https://doi.org/10.1038/nclimate1495)
- Turner AG, Inness PM, Slingo JM (2007) The effect of doubled CO₂ and model basic state biases on the monsoon-ENSO system. I: mean response and interannual variability. *Q J R Meteorol Soc* 133(626):1143–1157. doi:[10.1002/qj.82](https://doi.org/10.1002/qj.82)
- Wang B, Liu J, Kim H-J, Webster PJ, Yim S-Y, Xiang B (2013) Northern hemisphere summer monsoon intensified by mega-El Niño/southern oscillation and Atlantic multidecadal oscillation. *Proc Natl Acad Sci* 110(14):5347–5352
- Webster PJ, Fasullo J (2003) MONSOON: dynamical theory. In: *Encyclopedia of atmospheric sciences*. Academic Press, pp 1370–1386. doi:[10.1016/b0-12-227090-8/00236-0](https://doi.org/10.1016/b0-12-227090-8/00236-0)
- Wu G, Liu Y, He B, Bao Q, Duan A, Jin F-F (2012) Thermal controls on the Asian summer monsoon. *Sci Rep* 2. doi:[10.1038/srep00404](https://doi.org/10.1038/srep00404)
- Wu P, Christidis N, Stott P (2013) Anthropogenic impact on earth's hydrological cycle. *Nat Clim Change* 3(9):807–810. doi:[10.1038/nclimate1932](https://doi.org/10.1038/nclimate1932)
- Xie S-P, Xu H, Saji NH, Wang Y, Liu WT (2006) Role of narrow mountains in large-scale organization of Asian monsoon convection. *J Clim* 19(14):3420–3429. doi:[10.1175/JCLI3777.1](https://doi.org/10.1175/JCLI3777.1)
- Yatagai A, Kamiguchi K, Arakawa O, Hamada A, Yasutomi N, Kito A (2012) APHRODITE: constructing a long-term daily gridded precipitation dataset for Asia based on a dense network of rain gauges. *Bull Am Meteorol Soc* 93(9):1401–1415. doi:[10.1175/BAMS-D-11-00122.1](https://doi.org/10.1175/BAMS-D-11-00122.1)